JOURNAL OF THERMOPHYSICS AND HEAT TRANSFER
Vol. 21, No. 4, October–December 2007

Validation of Local Similarity Solutions to Conjugate Free Convection for Vertical Plate

Vipin Yadav*
The University of Auckland, Auckland 1142, New Zealand
and
Keshav Kant†
Indian Institute of Technology, Kanpur, India 208 016

DOI: 10.2514/1.27715

The paper presents the local similarity solution for a vertical heated plate subjected to conjugate free convection. A part of the surface is subjected to uniform heat flux and rest under uniform wall temperature conditions. The fractional areas under uniform heat flux and uniform wall temperature conditions are considered variable. The possible solutions based on thermally thin wall regime approximation were investigated and found to satisfactorily deal with longitudinal conduction and temperature variation in a transverse direction. A test setup was developed and the experiments were conducted to obtain relevant data for comparison with the analytical solutions. The approximate range of the Rayleigh number during various test conditions was 2.7×10^8 to 5.4×10^8, and the order of magnitude of the heat conduction parameter (α) was between 10^{-3} and 1. Limiting solutions under considered thermal and geometric conditions are analyzed in detail, and comparison with experimental data is presented. Reasonable agreement is observed between the experimental and analytical results.

Nomenclature

b	=	distance between heated plate and insulated wall
c	=	specific heat, kJ/kg · K
f	=	nondimensional stream function
g	=	acceleration due to gravity, m/s^2
H	=	height of plate, m
k	=	thermal conductivity of fluid, kJ/m^2 · K
Pr	=	Prandtl number
p	=	pressure, Pa
Ra	=	Rayleigh number
T	=	temperature, °C
t	=	plate thickness, m
u, v	=	x, y velocity component
x, y	=	Cartesian coordinate
z	=	nondimensional normal coordinate to the strip
α	=	heat conduction parameter
β	=	volumetric expansion coefficient
Γ_0	=	fluid nondimensional temperature at the strip
γ	=	dimensionless surface temperature
δ	=	boundary layer thickness, m
ε	=	aspect ratio of the plate (h/L)
η	=	nondimensional normal coordinate for the flow
θ	=	nondimensional temperature for fluid
μ	=	dynamic viscosity, kg/m · s
ν	=	kinematic viscosity, m^2/s
ρ	=	density of fluid, kg/m^3
χ	=	nondimensional longitudinal coordinate
ψ	=	surface heat generation, W/m^2
$\bar{\psi}$	=	average heat generation over the surface, W/m^2

Subscripts

a	=	wall
a, norm	=	normalized quantity
c	=	characteristic
∞	=	ambient
max	=	maximum value

I. Introduction

THE conjugate heat transfer mechanism due to natural convection at the surface and conduction below is relevant for many heat transfer processes, for example, for the cases like printed circuit boards mounted with heat generating component arrays, multilayered air cooled heat exchangers and plate heaters, and so on. A thorough analysis of mechanism is important for predicting the intensity of thermally induced mechanical stresses in the bodies subjected to conduction and convection simultaneously.

Vallejo and Trevino [1] presented an analytical study for the cooling of a flat plate in a convective flow accounting for the longitudinal heat conduction. It was found that for large but finite thermal conductivity of the plate, the temperature adjusts itself to a pseudoequilibrium condition and further evolution of the plate temperature slows down. Mendez and Trevino [2] performed theoretical investigation to study heat transfer characteristics of a thin vertical strip with internal heat generation. It was concluded that to avoid excessive thermal stresses inside the material under mentioned circumstances a natural-convection process must be used with caution. Naylor et al. [3] studied two-dimensional laminar free convection between isothermal vertical plates. It was shown that a full elliptic solution gave more accurate values of local heat transfer quantities when compared with boundary layer equations, especially in the entrance region. Yadav and Kant [4] presented an experimental and numerical study for several different combinations of uniform heat flux and uniform wall temperature heating conditions on a single surface under buoyancy assisted convection cooling. Empirical expressions for an averaged Nusselt number for the considered values of thermal and flow parameters were developed. Trevino and Linan [5] studied the steady-state and transient processes of the external heating of a plate under a convective flow with the inclusion of the axial heat conduction through the plate using perturbation methods. Chen et al. [6] analyzed laminar free convection along horizontal, inclined, and vertical flat plates with power-law variation

Received 8 September 2006; revision received 11 April 2007; accepted for publication 3 May 2007.

*Post Doctoral Fellow, Department of Mechanical Engineering, School of Engineering; v.yadav@auckland.ac.nz.

†Professor (retired), Department of Mechanical Engineering; keshav@iitk.ac.in (Corresponding Author).

of the wall temperature or of the surface heat flux. Kazansky et al. [7] studied natural-convection heat transfer from a vertical electrically heated plate, which is symmetrically placed in a chimney of variable height. They analyzed the dependence of the temperature distribution on the flow field. Sparrow et al. [8] described a combined experimental and analytical/numerical study of turbulent mass (or heat) transfer in a flat, rectangular duct with streamwise periodic, nonuniform mass (heat) transfer at one of the principal walls. Chen et al. [9] investigated the natural-convection heat transfer coupled with the effect of thermal conduction from a steel plate with discrete sources. The average heat transfer was correlated from the experimental data as the function of the relative heating space and Rayleigh number. Pozzi and Lupo [10] studied the integral thermo-fluid-dynamic field resulting from the coupling of natural convection along and conduction inside a heated flat plate by means of expansions based on the Pade approximant technique and asymptotic solutions. Merkin and Pop [11] developed the technique for nondimensionalization of governing equations for conjugate-free convection boundary layer flows over a vertical plate. A self-developed efficient finite difference scheme was used to solve the flow equations and it was shown that the asymptotic expansion gave reliable results even at moderate values of dimensionless distance along the plate.

The current work investigates the conjugate heat transfer problem for a vertical heated plate subjected to natural convection at the surface and conduction below. The lower part of the total heated surface is kept at uniform heat flux (UHF) and the upper section at uniform wall temperature (UWT) conditions. The effective surface areas under two conditions are taken variable. Analytical solutions for dimensionless temperature and heat flux profiles are obtained based on thermally thin wall regime approximation. Subsequently, experiments are conducted to obtain relevant data for comparison purpose. The Rayleigh number (Ra) is kept between 2.7×10^8 and 5.4×10^8 and the order of magnitude for heat conduction parameter (α) between 10^{-3} and 1. The analytical results and experimental data are compared and trends are analyzed in detail.

II. Analytical Solution

Consider a flat plate, oriented vertically, with front surface subjected to natural-convection cooling and thermally insulated at back. Lower right corner of the plate is at the origin of Cartesian coordinate system with x-axis pointing upwards in the longitudinal direction and y-axis is normal to the surface (see Fig. 1); height and thickness of the plate are H and t, respectively.

The thermal condition at the plate surface is a combination of UHF and UWT conditions corresponding to the vertical lengths rH and $(1-r)H$, respectively. Such a thermal condition is expected to result in the development of a viscous nonisothermal boundary layer [2] at the vertical surface. To determine the representative boundary layer thickness, assume a characteristic temperature T_c at the plate surface and the associated characteristic temperature difference $\Delta T_c = (T_c - T_\infty)$. The Rayleigh number and the order of magnitudes of boundary layer thickness, induced velocity, and heat flux across the fluid are given as [2]

$$Ra_c = \frac{g\beta \Delta T_c H^3}{\nu^2} Pr; \qquad \delta \sim \frac{H}{Ra_c^{0.25}} \left(\frac{\Delta T_c}{\Delta T}\right)^{0.25}$$
$$u_c \sim \frac{Ra_c^{0.5}\nu}{Pr\,H} \left(\frac{\Delta T}{\Delta T_c}\right)^{0.5}; \quad \text{and} \quad q = \frac{k(\Delta T)^{1.25} Ra_c^{0.25}}{H(\Delta T_c)^{0.25}} \tag{1}$$

Let ψ be the local surface heat generation then the average surface heat generation is

$$\bar{\psi} = \frac{1}{H}\int_0^L \psi \, dx \tag{2}$$

Based upon characteristic normal temperature drop ΔT_a, thermal energy generated inside the plate is given as

$$e = \frac{k_a \Delta T_a}{t} \sim \bar{\psi} \cdot t \tag{3}$$

Because conduction and convection are the only means of energy transfer, Eqs. (2) and (3) give

$$\frac{(\Delta T)^{1.25}}{(\Delta T_c)^{0.25}} Ra_c^{0.25} \sim \frac{tH}{k}\bar{\psi} \tag{4}$$

As only the order of magnitude is considered, the analysis will not be affected if the order of magnitudes of ΔT_c and ΔT are taken the same. Thus

$$\Delta T_c Ra_c^{0.25} \sim \frac{tH}{k}\bar{\psi} \tag{5}$$

The nondimensional longitudinal heat conductance of the strip is defined by $\alpha = k_a t/kHRa_c^{0.25}$, and aspect ratio by $\varepsilon = t/H$. The necessary condition for the thermally thin wall regime is $\alpha/\varepsilon^2 \gg 1$. Therefore

$$\Delta T_c/\Delta T_a \sim \alpha/\varepsilon^2 \Rightarrow \Delta T_c \gg \Delta T_a$$

We consider steady-state laminar natural-convection flow with constant thermophysical properties. After the use of Boussinesq approximation, the governing equations for the problem can be written as [11]

$$\left.\begin{aligned} &\tfrac{\partial u}{\partial x} + \tfrac{\partial v}{\partial y} = 0 \\ &u\tfrac{\partial u}{\partial x} + v\tfrac{\partial v}{\partial y} = g\beta(T - T_\infty) + \nu\tfrac{\partial^2 u}{\partial y^2} \\ &u\tfrac{\partial T}{\partial x} + v\tfrac{\partial T}{\partial y} = \tfrac{\nu}{Pr}\tfrac{\partial^2 T}{\partial y^2} \end{aligned}\right\} \tag{6}$$

Here, u and v are the velocity components in x and y directions; T is the temperature of fluid and ν and Pr are the kinematic viscosity and the Prandtl number, respectively. Assuming dimensional and nondimensional stream functions as Ψ and f respectively, we now introduce the following nondimensional independent variables

$$\chi = \frac{x}{H}, \qquad \eta = Ra_c^{0.25}\frac{y}{H\chi^{0.25}}, \qquad z = \frac{y}{t}$$
$$f = \frac{Pr\Psi}{\nu Ra_c^{0.25}\chi^{0.75}}, \qquad \theta = \frac{T - T_\infty}{\Delta T_c}, \qquad \theta_a = \frac{T_a - T_\infty}{\Delta T_c} \tag{7}$$

The nondimensional boundary layer flow equations for large values of Rayleigh number can be written as [11]

$$\frac{\partial^2\theta}{\partial\eta^2} + \frac{3}{4}f\frac{\partial\theta}{\partial\eta} = \chi\left(\frac{\partial f}{\partial\eta}\frac{\partial\theta}{\partial\chi} + \frac{\partial f}{\partial\chi}\frac{\partial\theta}{\partial\eta}\right) \tag{8}$$

$$\frac{\partial^3 f}{\partial\eta^3} + \theta = \frac{1}{Pr}\left[\frac{1}{2}\left(\frac{\partial f}{\partial\eta}\right)^2 - \frac{3}{4}f\frac{\partial^2\theta}{\partial\eta^2} + \chi\left(\frac{\partial f}{\partial\eta}\frac{\partial^2 f}{\partial\chi\partial\eta} - \frac{\partial f}{\partial\chi}\frac{\partial^2 f}{\partial\eta^2}\right)\right] \tag{9}$$

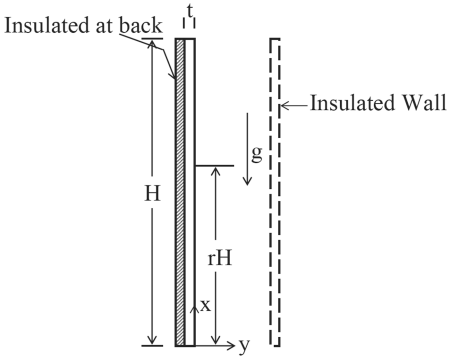

Fig. 1 Schematics of heated plate in vertical channel

$$\alpha\frac{\partial^2\theta_a}{\partial\chi^2}+\frac{\alpha}{\varepsilon^2}\frac{\partial^2\theta_a}{\partial z^2}+\frac{\psi}{\bar{\psi}}=0 \tag{10}$$

Let us consider rH length of plate having UHF condition and remaining $(1-r)H$ having UWT over the surface $(0<r<1)$. For UHF condition heat generation below the surface must be spatial constant.

$$\text{Let}\ \ \psi=\pi \tag{11}$$

$$\therefore\ \bar{\psi}=\frac{1}{H}\int_0^H \pi\,\mathrm{d}x=\pi \tag{12}$$

Therefore Eq. (8) takes the form

$$\alpha\frac{\partial^2\theta_a}{\partial\chi^2}+\frac{\alpha}{\varepsilon^2}\frac{\partial^2\theta_a}{\partial z^2}+1=0 \tag{13}$$

For the UWT surface, let $T_w=\tau$

$$\theta_w=\frac{\tau-T_\infty}{\Delta T_c}=\gamma \tag{15}$$

As τ and γ are not a function of χ, therefore Eq. (11) takes the form

$$\frac{\alpha}{\varepsilon^2}\frac{\partial^2\theta_a}{\partial z^2}+\frac{\psi}{\bar{\psi}}=0 \tag{16}$$

We need to solve Eqs. (8), (9), and (13) for the range $0<\chi\le r$ subjected to boundary conditions

$$\text{at}\ \ \eta=0,\quad z=0\quad f=\frac{\partial f}{\partial\eta}=0,\quad \theta=\theta_a,\quad \frac{\partial\theta}{\partial\eta}=\frac{\alpha\chi^{0.25}}{\varepsilon^2}\frac{\partial\theta_a}{\partial z} \tag{17}$$

$$\text{for}\ \ z=-1\qquad \frac{\partial\theta_a}{\partial z}=0 \tag{18}$$

$$\text{for}\ \ \eta\to\infty\qquad \frac{\partial f}{\partial\eta}=\theta_a=0 \tag{19}$$

$$\text{for}\ \ \chi=0\frac{\partial\theta_a}{\partial\chi}=0 \tag{20}$$

For the range $r<\chi<1$, we need to solve Eqs. (8), (9), and (16) subjected to the boundary conditions shown by Eqs. (17–19) and

$$\theta_a=\gamma,\qquad \frac{\partial\theta_{a1}}{\partial\chi}=0\quad \text{for}\ \ \chi=r \tag{21}$$

To determine the solution for the case $\alpha\to\infty$, consider a general function Θ corresponding to properties of fluid like f and θ, assume following two series

$$\theta_a=\sum_{j=0}^{\infty}\frac{1}{\alpha^j}\theta_{a,j}(\chi)\quad\text{and}\quad \Theta=\sum_{j=0}^{\infty}\frac{1}{\alpha^j}\Theta_{a,j}(\chi) \tag{22}$$

For the range $0<\chi\le r$:

Integrating Eq. (13) along the normal coordinate we get

$$\alpha\frac{\partial^2\theta_a}{\partial\chi^2}z+\frac{\alpha}{\varepsilon^2}\frac{\partial\theta_a}{\partial z}+z=F_1(\chi,\theta) \tag{23}$$

F_1 is a function governed by boundary conditions.

Substituting Eqs. (18), (19), and (21) as boundary conditions in Eq. (23) we get

$$\alpha\frac{\partial^2\theta_a}{\partial\chi^2}=-\left(\chi^{-0.25}\frac{\partial\theta}{\partial\eta}\bigg|_0+1\right) \tag{24}$$

Substituting Eq. (22) into Eq. (24) we get,

$$\begin{cases}\frac{\partial^2\theta_{a0}}{\partial\chi^2}=0\\ \frac{\partial^2\theta_{a1}}{\partial\chi^2}=-\left(\chi^{-0.25}\frac{\partial\theta_0}{\partial\eta}\Big|_0+1\right)\\ \frac{\partial^2\theta_{aj}}{\partial\chi^2}=-\chi^{-0.25}\frac{\partial\theta_{j-1}}{\partial\eta}\Big|_0\end{cases} \tag{25}$$

This set of equations is to be solved using the adiabatic boundary condition

$$\frac{\partial\theta_{aj}}{\partial\chi}=0\quad\text{at}\ \ \chi=0\quad\text{for the entire range of}\ j \tag{26}$$

For the range $r<\chi\le 1$, Eq. (23) is to be replaced by

$$\frac{\alpha}{\varepsilon^2}\frac{\partial\theta_a}{\partial z}+\frac{\psi}{\bar{\psi}}z=F_2(\chi,\theta) \tag{27}$$

F_2 is a function governed by boundary conditions.

Using Eq. (18) in Eq. (27) we get

$$\frac{\alpha}{\varepsilon^2}\frac{\partial\theta_a}{\partial z}+\frac{\psi}{\bar{\psi}}(z+1)=0 \tag{28}$$

Now, using Eq. (16) in Eq. (27), we get

$$\frac{\psi}{\bar{\psi}}=-\chi^{-0.25}\frac{\partial\theta}{\partial\eta}\bigg|_0 \tag{29}$$

Here, the leading variable θ_{a0} is a constant [12].

$$\frac{\partial\theta}{\partial\eta}\bigg|_0=-\Gamma_0\theta_{a0}^{1.25}=-0.75 \tag{30}$$

Γ_0 is a function of fluid Prandtl number [2] and given as

$$\Gamma_0(Pr)\approx 0.75\left(\frac{0.4Pr}{1+2Pr^{0.5}(1+Pr^{0.5})}\right)^{0.25} \tag{31}$$

$$\Rightarrow\ \theta_{a0}=\left(\frac{3}{4\Gamma_0(Pr)}\right)^{0.8} \tag{32}$$

For the UWT surface, using Eq. (30) in Eq. (29) we get

$$\frac{\psi}{\bar{\psi}}=\chi^{-0.25}\Gamma_0\theta_{a0}^{1.25}=0.3852\gamma^{1.25}\chi^{-0.25} \tag{33}$$

$$\bar{\psi}=2.596\gamma^{-1.25}\chi^{0.25}\psi \tag{34}$$

Thus if we can know local heat generation at some point on the plate surface in the region $r<\chi\le 1$, it is possible to estimate mean heat generation for the entire region.

By the definition of $\bar{\psi}$ we have

$$\bar{\psi}\,\mathrm{d}\chi+(1-r)\,\mathrm{d}\bar{\psi}=\psi\,\mathrm{d}\chi\qquad \psi=(1-r)\bar{\psi}+\frac{\mathrm{d}\bar{\psi}}{\mathrm{d}\chi}$$

Using Eq. (34) we have

$$\frac{\mathrm{d}\psi}{\psi}=[0.385\gamma^{1.25}\chi^{-0.25}-(1-r)-0.25\chi]\,\mathrm{d}\chi$$

The integral solution for the above is

$$\psi=\psi_0\cdot e^{0.513\gamma^{1.25}\chi^{0.75}-(1-r)\chi-0.125\chi^2} \tag{35}$$

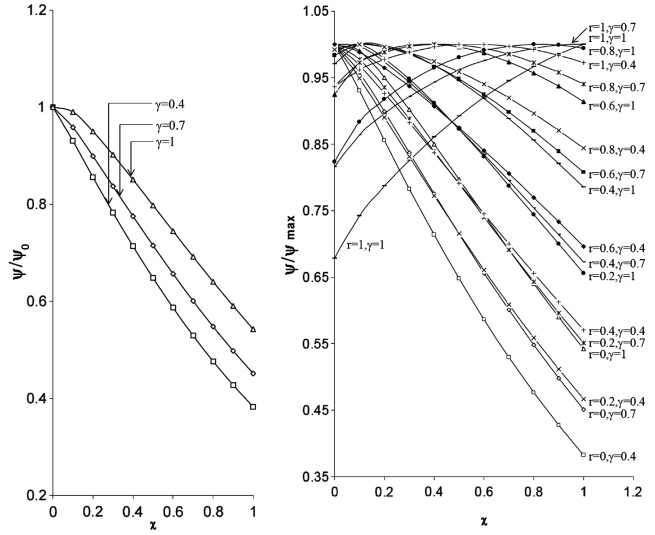

a) b)

Fig. 2 a) Variation of normalized heat flux ψ/ψ_0 along the plate height [for Eq. (35)]; b) comparison of normalized heat flux along the plate height for different values of UWT/UHF fraction r and dimensionless mean temperature γ.

ψ_0 is an integration constant and can be calculated by assuming

$$\psi = 1 \quad \text{for } \chi = r \quad \text{and} \quad \gamma = 0 \tag{36}$$

Applying the above condition up on Eq. (35) we get

$$\psi_0 = e^{r(1-0.875r)} \tag{37}$$

Trends for heat flux ratio ψ/ψ_0 as the function of the plate height and different values of dimensionless mean temperature γ are shown in Fig. 2a. Figure 2b compares normalized heat flux for different values of the UWT/UHF fraction r and γ. The values of $\psi/\psi_{\max}$ corresponding to χ beyond the range $r < \chi \leq 1$ also appear but to be disregarded. Three types of curves are observed as described below:

a) Those originating at unity, the value of $\psi/\psi_{\max}$ reduces monotonically as χ increases, for example, those corresponding to $r = 0$, $\gamma = 0.4$ and $r = 0.2$, $\gamma = 0.4$;

b) Those beginning with intermediate values of $\psi/\psi_{\max}$, however, attaining unity for some $r < \chi < 1$ before ending up again at some intermediate ordinate value; for example, those corresponding to $r = 0.4$, $\gamma = 1$ and $r = 0.6$, $\gamma = 0.4$; and

c) Those monotonically terminating at unity; for example, those corresponding to $r = 0.8$, $\gamma = 1$ and $r = 1$, γ=1.

For the UHF surface, using Eq. (32) in Eq. (25) we get

$$\frac{\partial^2 \theta_{a1}}{\partial \chi^2} = \chi^{-0.25}\Gamma_0 \theta_{a0}^{1.25} - 1 \tag{38}$$

When Eq. (38) is subjected to boundary conditions in Eq. (26), the following first order solution results:

$$\theta_{a1} = \zeta_0 + \zeta_1 \chi + \zeta_2 \chi^2 + \zeta_3 \chi^{7/4} \tag{39}$$

Here $\zeta_1 = 0$ due to Eq. (26); $\zeta_2 = -0.5$ and $\zeta_3 = \frac{16}{21}\Gamma_0 \theta_{a0}^{1.25} = 0.57$. ζ_0 can be chosen based upon flux distribution over the plate in the region $0 < \chi \leq r$. Now Eqs. (21) and (39) give

$$\theta_{a1} = \frac{\gamma}{(0.57 r^{-0.25} - 0.50).r^2} - 0.50\chi^2 + 0.57\chi^{7/4} \tag{40}$$

The average nondimensional temperature over the entire plate surface (up to the term of order $1/\alpha$) can be given by

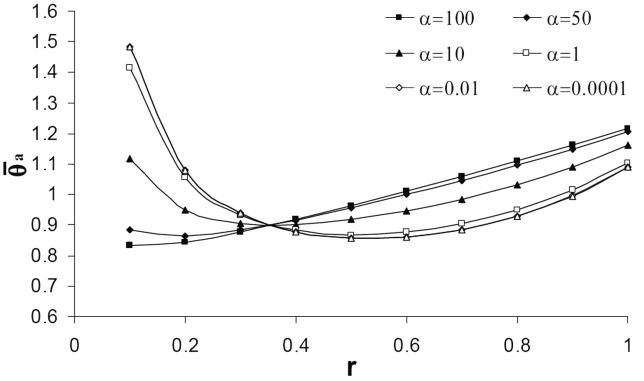

Fig. 3 Comparison of leading order solution for average nondimensional temperature at the plate surface as function of fraction r and thermal diffusivity α with $\gamma = 1.0$.

$$\begin{aligned}\bar{\theta}_a &= \int_0^r \theta_a \, \mathrm{d}\chi + \int_r^1 \theta_a \, \mathrm{d}\chi = \left(\theta_{a0} + \frac{1}{\alpha}\bar{\theta}_{a1}\right) r + \gamma(1-r) \\ &= \left[1.704 + \frac{1}{\alpha}\left(\frac{\gamma}{(0.57 r^{-0.25} - 0.50) r^2} \right.\right. \\ &\quad \left.\left. - 0.166 r^2 + 0.207 r^{7/4}\right)\right] r + \gamma(1-r) \\ &= \frac{\gamma}{(0.57 r^{-0.25} - 0.50) r\alpha} + \gamma + (1.704 - \gamma) r \\ &\quad + \frac{0.207 r^{11/4}}{\alpha} - \frac{0.166 r^3}{\alpha}\end{aligned} \tag{41}$$

Figure 3 presents the comparison of trends in leading order solution for average nondimensional temperature at the plate surface for different values of UWT/UHF fraction r and thermal parameter α. For α with order one or less, $\bar{\theta}_a$ has a tendency to start with a value above unity, and as r increases it drops rapidly until $r = 0.37$, and then gradually rises with a further increase in r. The slope of the curve in the first (decreasing) phase has a limiting value that corresponds to $\alpha = 1$; all the curves show concavity upwards in the second (rising) phase. For the curves corresponding to α with order higher than unity, the slope in the first phase is less when compared with previously discussed cases; during the next phase ($r > 0.37$) the slope vanishes and $\bar{\theta}_a$ attains a linear relation with r.

The effect of variation in γ and α, upon the trends in r vs $\theta_{a,\text{norm}}$ is shown in Fig. 4. $\theta_{a,\text{norm}}$ is the normalized value of $\bar{\theta}_a$. For $O(\alpha) > 1$, $\theta_{a,\text{norm}}$ vs r curves show typical drop and rising phases in succession. With the increase in γ, the first phase extends up to larger r. The lowest value of $\theta_{a,\text{norm}}$ lies in the first quarter of the range for r.

Observation of trends in r vs $\theta_{a,\text{norm}}$ curves indicates up to 2.5 times larger $\theta_{a,\text{norm}}$ at the end of the second phase as compared with the onset of the first phase. The described features are prominently observed in Figs. 4a–4c. The observation of trends in r vs $\theta_{a,\text{norm}}$ curves in Figs. 4d–4f indicate a 27% reduced $\theta_{a,\text{norm}}$ at the end of the second phase as compared with that at the onset of first phase; also, the lowest $\theta_{a,\text{norm}}$ values lie beyond the first quarter of the range for r values. Curves associated with a small γ are found to have a successively reducing slope in the rising (second) phase as $\mathcal{O}(\alpha) < 1$. No significant difference is observed between trends in Figs. 4e and 4f, which means that there will be an insignificant variation in pattern for $\theta_{a,\text{norm}}$ vs r curves when $\mathcal{O}(\alpha) < 10^{-4}$.

To determine the solution for the case $\alpha \to 0$, for the range $0 < \chi \leq r$, Eq. (13) is replaced by

$$\frac{\alpha}{\varepsilon^2}\frac{\partial^2 \theta_a}{\partial z^2} + 1 = 0 \tag{42}$$

Substituting Eqs. (18) and (19) as a boundary condition, Eq. (42) reduces to

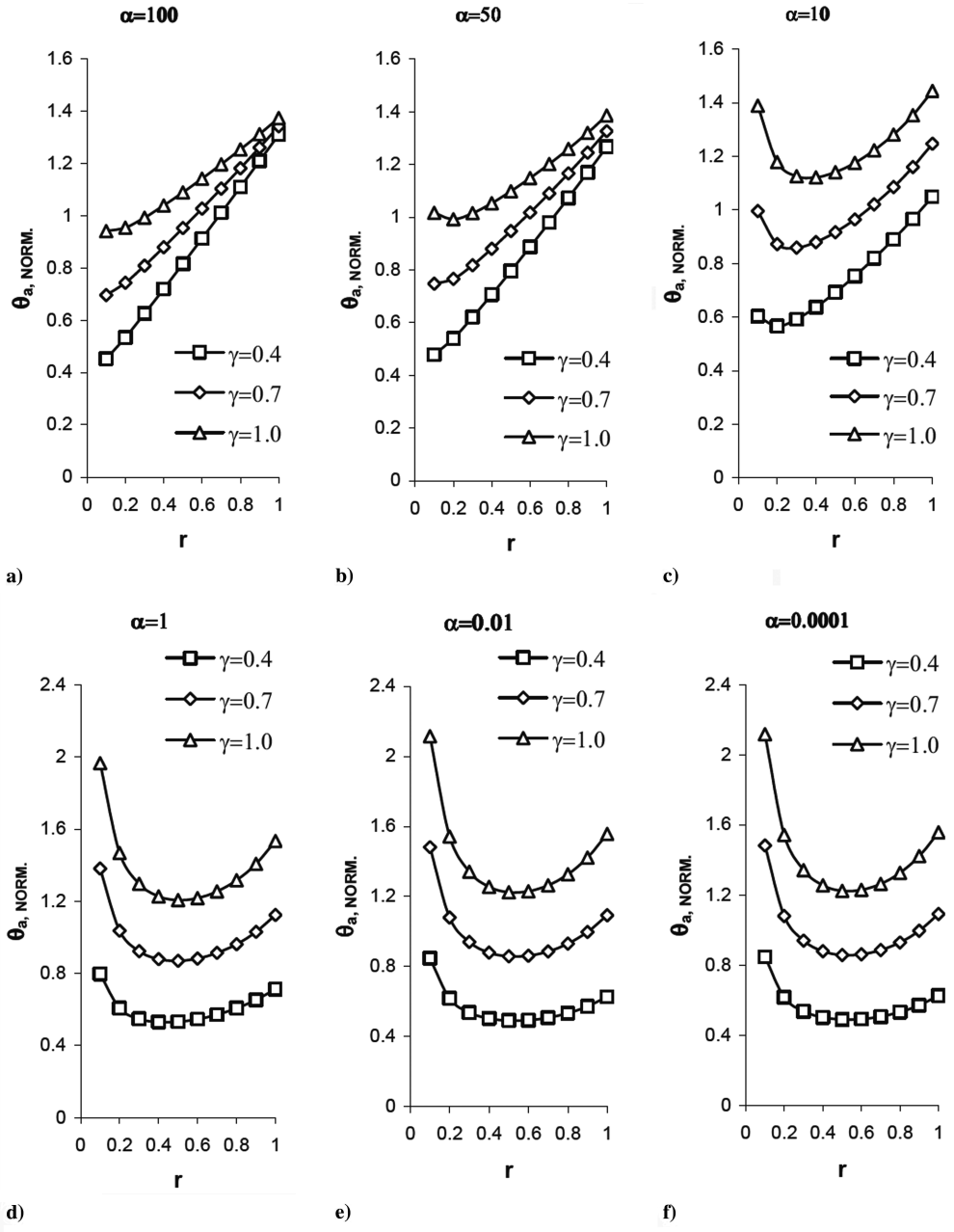

Fig. 4 Comparison of normalized first order solution for nondimensional temperature $\theta_{a,\text{norm}}$ as function of r for different α and γ.

$$\chi^{-0.25}\left.\frac{\partial\theta_0}{\partial\eta}\right|_0 = -1 \tag{43}$$

For this particular case the possible solution is in the form

$$\theta_a = \theta_0'\chi^{0.2} \tag{44}$$

For getting $\bar{\theta}_0$ we need to make the following substitution in Eqs. (8) and (9):

$$\begin{aligned} \eta &= \chi^{-0.05}\eta', \qquad f = \chi^{0.05}f' \\ \theta &= \chi^{0.2}\theta', \quad \text{and} \quad \theta_a = \chi^{0.2}\theta_0' \end{aligned} \tag{45}$$

As a result, we get

$$\frac{\partial^2\theta'}{\partial\eta'^2} + \frac{4}{5}f'\frac{\partial\theta'}{\partial\eta'} - \frac{1}{5}\theta'\frac{\partial f'}{\partial\eta'} = 0 \tag{46}$$

$$\frac{\partial^3 f'}{\partial\eta'^3} + \theta' = \frac{1}{Pr}\left[\frac{3}{5}\left(\frac{\partial f'}{\partial\eta'}\right)^2 - \frac{4}{5}f'\frac{\partial^2\theta'}{\partial\eta'^2}\right] \tag{47}$$

These are to be solved subjected to the following boundary conditions:

$$\text{at } \eta' = 0, \qquad f' = \frac{\partial f'}{\partial\eta'} = 0, \qquad \frac{\partial\theta'}{\partial\eta'} = -1 \tag{48}$$

$$\text{for } \eta' \to \infty \qquad \frac{\partial f'}{\partial\eta'} = \theta_a' = 0 \tag{49}$$

To apply the finite difference method, the following expressions are used:

$$f_{k+1} = f_{k-1} + A_k\frac{\theta_{k+1}}{\theta_k} + B_k\frac{\theta_{k+1}}{\theta_k} - C_k \tag{50}$$

where

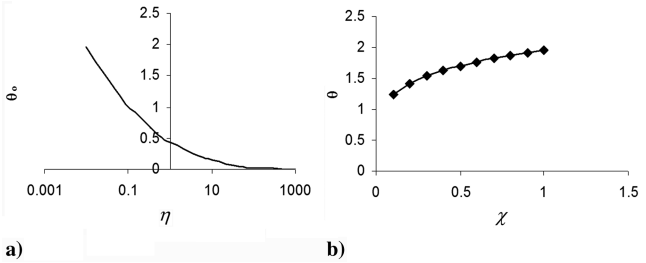

Fig. 5 a) Variation of θ_0 with nondimensional normal coordinate at the plate surface; b) dimensionless temperature vs nondimensional plate height.

$$A_k = 4f_k + \frac{10}{\Delta\eta_{k+1}}$$

$$B_k = \frac{10}{\Delta\eta_{k+1}} - 4f_k \quad \text{and} \quad C_k = 10\cdot\left(\frac{1}{\Delta\eta_{k+1}} + \frac{1}{\Delta\eta_k}\right) \tag{51}$$

$$\theta_{k+1} = -D_k\theta_{k-1} + (D_k+1)\theta_k + E_k\frac{(f_{k+1}-f_{k-1})^2}{f_k} + F_k\frac{f_{k+1}}{f_k} + G_k\frac{f_{k-1}}{f_k} + H_k$$

Also,

$$D_k = \frac{\Delta\eta_{k+1}}{\Delta\eta_k}; \qquad E_k = \frac{15D_k}{32(1+D_k)}$$

$$F_k = \frac{5Pr}{4\Delta\eta_k} \quad \text{and} \quad G_k = \frac{5Pr\cdot D}{4\Delta\eta_k}\left(\frac{\Delta\eta_k + \Delta\eta_{k+1}}{\Delta\eta_{k-1}}\right)$$

In addition to the above, forward difference and backward difference expressions were substituted in place of the central difference to ensure the implementation of boundary conditions.

Successive iterations are used for $k = 0, 1, 2 \ldots N$. N represented the value such that

$$|f_N - f_{N-1}| < \varepsilon_1 \quad \text{and} \quad |\theta_N - \theta_{N-1}| < \varepsilon_2$$

Values of ε_1 and ε_2 were kept sufficiently close to zero.

For the case of air ($Pr = 0.72$), $\theta_0' \approx 1.95$ has been obtained. The variation of θ_0 with a nondimensional normal coordinate at the plate surface is shown in Fig. 5a; Fig. 5b shows the variation in dimensionless temperature with the increase in nondimensional plate height.

Now we consider the range $r < \chi \leq 1$.

Using $\alpha = 0$ and $(\partial^2\theta_a/\partial z^2) = 0$ in Eq. (10) we have

$$\psi \approx 0 \tag{52}$$

This means there is negligible heat generation in this portion of the plate; no analytical solution is possible under such circumstances.

III. Experimentation

A. Experimental Setup

The experimental setup was designed to obtain necessary data from the surface of a plate in a channel-like configuration with the dimensions sufficiently larger than the theoretical boundary layer thickness. The setup consisted of a test section and intake unit as shown in Fig. 6. The test section was a rectangular duct oriented vertically and having a provision for holding two vertical plates in parallel; a lead screw mechanism was provided to move these nearer or apart in such a way that the region formed in-between remained symmetrically placed. The test section was 700 mm high with 300×200 mm lateral dimensions. To facilitate panoramic viewing inside the unit, shatter resistant (plate safety) glass material with specified thermal conductivity 3.7 W/m · K (approximately) was used for construction. The test configuration comprised heated regions of total vertical length 500 mm and a downstream unheated

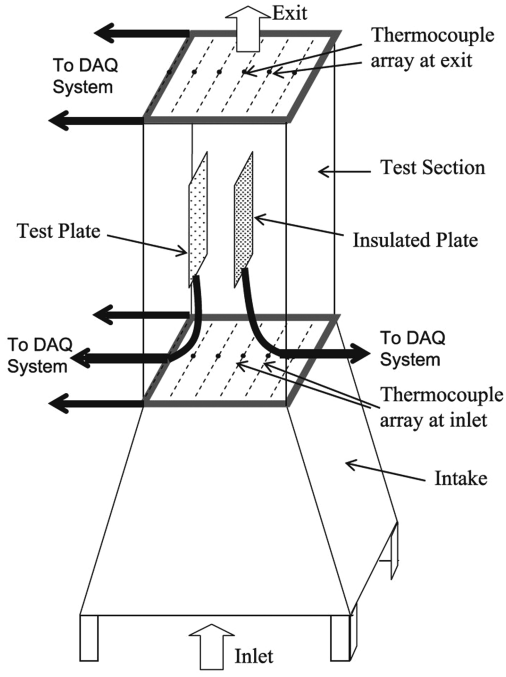

Fig. 6 Schematic of the experimental setup.

region of length 100 mm. The heated regions were divided into five heated zones appearing one after another in channel formed in-between plate specimen and insulated wall. The maximum horizontal dimension of the region of interest was 80 mm. A separate heating unit was embedded in each section. The scheme for the heated plate design is shown in Fig. 7.

Heat flux at the plate surface was obtained by measuring the temperature gradient across the plate thickness. The thermopiles were placed at both sides of the top plate. The difference in the temperature at the two surfaces was measured and used for calculating the temperature gradient and determining heat flux at the surface using the relation

$$Q = -k\frac{\Delta T}{\Delta x} \tag{53}$$

The UWT condition was simulated by selecting a material of high thermal conductivity (aluminum) for placing underneath the top plate. Under steady state, this denigrated the temperature gradients along the longitudinal direction of the top plate; a maximum of 0.21% temperature difference was observed at two ends of the top plate (along the flow direction), whereas the mean temperature at the surface was maintained near or below 100°C. For simulating the

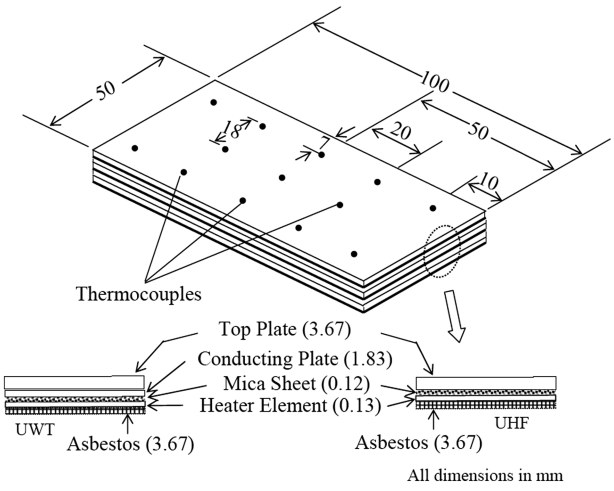

Fig. 7 Schematics for the heated plate.

UHF condition, it was ensured that the foil used in making the heating element was uniform in thickness (0.13 ± 0.001 mm) so that there was homogeneous resistance all over the heater surface area. Stainless steel foil was opted as a heater material with low thermal conductivity. During the experimentation, the maximum variation of heat flux for the UHF surface was found to be lower than 4%. The heated plate assembly was designed incorporating the flexibility of a comfortable replacement of the top plate. For experimentation purposes, aluminum, Teflon, and FR4 were used as the top plate material. The power supplied to each heater was monitored and precisely controlled separately, keeping basic dc accuracy near 0.025% for both voltage and current.

B. Measurement Methods Adopted

To conduct temperature measurement, *J*-type thermocouples prepared from 30-gauge Omega brand thermocouple wires were used. All the thermocouples with the help of extension wires were connected in a differential mode to the AMUX 64-T DAQ card from National Instruments. Measurements of temperatures were made by data acquisition through DAQ card No. PCI-6024E. For acquisition, storage, and analysis of the data, Lab VIEW software was used. Velocity measurement was also carried out, but manually using a vane anemometer at the exit of the test section. The zone surface temperature was monitored by an array of thermocouples as shown in Fig. 7.

Five thermocouples were used to measure the temperature near the upstream location of the heated zone, while another five thermocouples were located near the downstream location. The temperature at the middle of the zone surface was measured using three thermocouples. The ambient air temperature was measured by the same type of thermocouples located in the proximity of the leading edge of the channel. To evaluate conductive heat losses, five thermocouples were affixed to the rear surface of both the heated wall and insulated surface in their centerline, 10, 30, 50, 70, and 90 mm downstream of the inlet section. Thermocouple voltages were recorded to an accuracy of 1 μV. Each thermocouple was calibrated in a 0.01 K thermostatic bath by means of a reference standard thermometer. The calibration of the temperature measuring system showed an estimated precision of the thermocouple-readout system of ± 0.2 K. While maintaining two different kinds of thermal conditions (i.e., UHF and UWT) at the test plate, it was ensured that any sudden change in temperature or heat flux value does not occur. Therefore, the temperature selected for the UWT surface was such that the temperature at the beginning of the following UHF surface remained as close as possible to the preceding surface temperature.

IV. Results and Discussion

The dimensions of the plate specimen were held fixed and the variation in the heat conduction parameter was achieved by varying the top plate material. The experimental data were obtained for three materials, viz., aluminum, Teflon, and FR4 for which the values of heat conduction parameter (α) were 1.178, 1.09×10^{-3}, and 1.636×10^{-3}, respectively. The distance between the test plate and the insulated plate was kept sufficiently larger than the theoretically calculated order of magnitude for boundary layer thicknesses in the flow and thermal fields over the test plate. For the assumed thermal condition over the surface, the leading order analytical solution for the UHF case and average nondimensional temperature $\bar{\theta}_a$ up to the order $1/\alpha$ was obtained and used for comparison with experimental data. As extreme temperature gradients were expected to occur for the UHF condition [8,13] over the total surface (i.e., $r = 0$), therefore this was opted to quantify the variation in measured values due to the presence of an insulated wall. Three distances between the test plate and the insulated plate, that is, $b = 40$, 60, and 80 mm, were chosen. The normalized heat flux ψ/ψ_0 as a function of nondimensional longitudinal coordinate χ for three plate separations is shown in Fig. 8. The analytical results due to Eq. (35) are also presented. The value of *Ra* was kept near 5.4×10^8. For greater plate separation, ψ/ψ_0 values were found to be larger toward the lower edge of the plate as compared with those for smaller plate separation; however, the opposite trend is observed toward the upper edge. For various plate separations, all the data were found to lie within 7% of the mean value. The discrepancy between analytical and experimental data was found to be less than 6%.

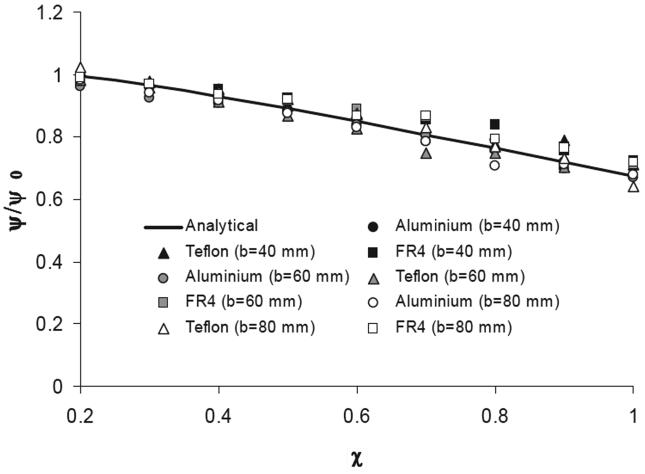

Fig. 8 Variation of normalized heat flux at the plate surface with an increase in nondimension distance over the surface from leading edge.

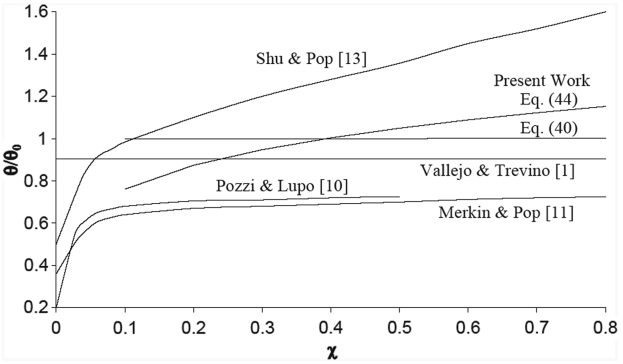

Fig. 9 Comparison of current work with data from the literature.

Figure 9 presents the comparison of analytical solutions due to Eqs. (40) and (44) (or $r = 0.8$ case) with the data from the literature. Both the analytical solutions are at the upper side of the data values due to Pozzi and Lupo [10] and Merkin and Pop [11]. The data due to Vallejo and Trevino [1] are in best agreement with the current work for maximum of the χ range; maximum deviation of near 10% and 15% occur for solutions due to Eqs. (40) and (44) respectively. The values due to Shu and Pop [14] start with the good agreement with current analytical solution, however, deviation up to 50% occurs at higher values of χ. The difference between the results for the current work and those from the literature is due to the difference in thermal and flow conditions at the surface.

Figure 10a shows the typical trends in experimental data when the initial $\frac{1}{5}$th portion of the plate surface was heated to UHF and the remaining portion was maintained at the UWT condition (i.e., $r = 0.2$) for the $\gamma = 0.2$ case. The analytical solution given by Eq. (35) is also presented for comparison. The values for ψ/ψ_0 are found to decrease with an increase in χ. The experimental values corresponding to Teflon as plate material are found nearest to the analytical solution. The experimental and analytical data for normalized heat generation (ψ/ψ_0) for all considered values of r and γ are presented in Table 1. The discrepancy between the analytical and experimental values is at a maximum (up to 10%) at $\gamma = 0.5$ and occurs near the upper end of the plate (see Table 1). The probable cause may be the inclusion of large disturbances in the natural convection flow pattern as the fluid progresses toward the upper edge of the test surface. The trends observed in Fig. 10b are for the largest

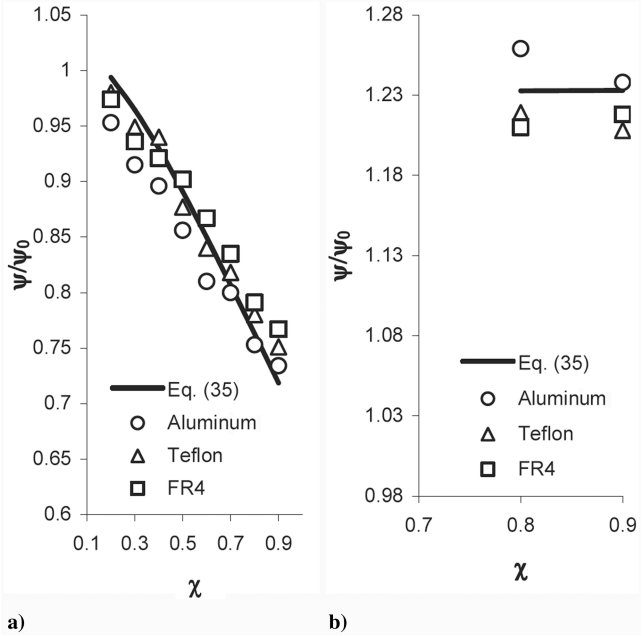

Fig. 10 Dependence of normalized heat generation under the plate surface upon the nondimensional plate height for $\gamma = 0.2$: a) $r = 0.2$ and b) $r = 0.8$.

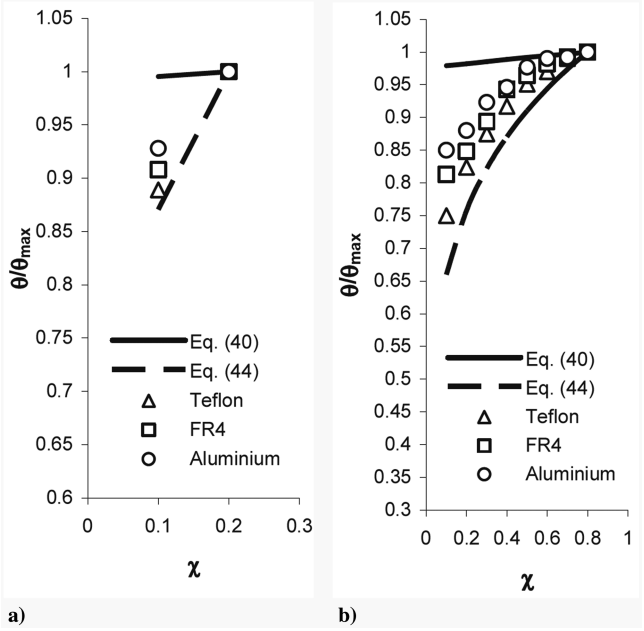

Fig. 11 Dependence of dimensionless surface temperature at the plate surface upon the nondimensional plate height for $\gamma = 0.2$ and a) $r = 0.2$ and b) $r = 0.8$.

considered value of r, that is, $r = 0.8$, and are not very conclusive as experimental data were available from two sets of thermocouples only at the surface with the UWT condition. The analytical trend is almost linear for all γ values, and the experimental data for FR4 appear in better agreement as compared with the other two materials. For $\gamma = 1.0$, ψ/ψ_0 values for all three materials lie at the higher side compared with analytical trends.

Trends of variation in normalized dimensionless surface temperature θ/θ_{max} as a function of χ at the plate surface under the UHF condition for the $r = 0.2$ and $\gamma = 0.2$ case, are shown in Fig. 11a. Experimental data are compared with the solution provided by Eqs. (40) and (44). For the lower value of γ, all the experimental data points lie between the analytical θ/θ_{max} value due to Eqs. (40) and (44); in general, there is a better agreement with the analytical results due to Eq. (44). The experimental and analytical data for dimensionless surface temperature (θ/θ_{max}) for all considered values of r and γ are presented in Table 2. It can be observed that at $\gamma = 0.5$ there is a shift in the experimental data from results due to Eq. (44). The experimental data for Teflon show more favor for analytical values due to Eq. (44), whereas the data for aluminum are nearer to the results due to Eq. (40). For $\gamma = 1.0$, least disagreement occurred for Teflon and FR4 data with the results due to Eq. (44). Apparently, the exact overlapping of experimental and analytical data values at $\chi = 0.2$ is due to normalization rather than the absolute lack of any discrepancy within the set of results. Figure 11b presents data for the case of $r = 0.8$ and $\gamma = 0.2$. In general, the slope in the χ vs θ/θ_{max} curve for Eq. (40) is found to reduce with the rise in γ; apparently a 50% reduction in slope occurs as γ increased from 0.2 to 0.5; followed by about a 40% reduction as γ increased from 0.5 to 1.0. The relative trends among the experimental data points for three different materials are not much affected by the increase in r from 0.4 to 0.8. The spread in the experimental data reduce from about 12% to

Table 1 Heat generation (ψ/ψ_0) at the plate for different values of γ.

		Normalized heat generation, ψ/ψ_0											
		$\gamma = 0.2$				$\gamma = 0.5$				$\gamma = 1.0$			
r	χ	Analytical	Experimental			Analytical	Experimental			Analytical	Experimental		
0.2	0.2	0.993	0.953	0.980	0.974	0.993	0.978	0.992	0.989	0.993	0.980	0.998	0.990
	0.3	0.964	0.915	0.949	0.936	0.964	0.941	0.969	0.954	0.964	0.956	0.980	0.968
	0.4	0.929	0.896	0.940	0.921	0.929	0.914	0.942	0.926	0.929	0.925	0.953	0.937
	0.5	0.890	0.856	0.877	0.902	0.890	0.875	0.889	0.907	0.890	0.889	0.910	0.911
	0.6	0.849	0.810	0.840	0.867	0.849	0.848	0.856	0.876	0.849	0.860	0.872	0.881
	0.7	0.806	0.800	0.818	0.835	0.806	0.805	0.826	0.842	0.806	0.821	0.849	0.842
	0.8	0.762	0.753	0.780	0.791	0.762	0.769	0.785	0.801	0.762	0.791	0.808	0.829
	0.9	0.718	0.734	0.751	0.767	0.718	0.743	0.754	0.769	0.718	0.764	0.780	0.792
0.4	04	1.007	1.008	0.997	0.978	1.007	1.013	1.001	0.989	1.000	1.017	1.011	0.999
	0.5	0.984	0.972	0.961	0.949	0.984	0.988	0.976	0.955	0.958	0.995	0.982	0.955
	0.6	0.957	0.968	0.949	0.938	0.957	0.974	0.958	0.950	0.913	0.978	0.938	0.950
	0.7	0.927	0.930	0.920	0.902	0.927	0.932	0.920	0.902	0.867	0.948	0.938	0.912
	0.8	0.895	0.913	0.907	0.883	0.895	0.914	0.907	0.883	0.820	0.926	0.907	0.888
	0.9	0.860	0.883	0.869	0.848	0.860	0.895	0.869	0.848	0.772	0.904	0.898	0.867
0.6	0.6	1.080	1.089	1.068	1.061	1.080	1.094	1.085	1.072	1.080	1.100	1.091	1.079
	0.7	1.067	1.071	1.059	1.050	1.067	1.085	1.069	1.056	1.067	1.095	1.083	1.061
	0.8	1.050	1.059	1.049	1.036	1.050	1.056	1.068	1.041	1.050	1.094	1.073	1.056
	0.9	1.029	1.039	1.047	1.026	1.029	1.049	1.047	1.020	1.029	1.072	1.062	1.044
0.8	0.8	1.232	1.259	1.219	1.210	1.232	1.263	1.246	1.236	1.232	1.272	1.258	1.250
	0.9	1.232	1.238	1.208	1.218	1.232	1.247	1.232	1.218	1.232	1.272	1.260	1.247

Table 2 Dimensionless surface temperature (θ/θ_{max}) at the plate surface for different values of γ.

		Dimensionless surface temperature, θ/θ_{max}														
		$\gamma = 0.2$					$\gamma = 0.5$					$\gamma = 1.0$				
		Analytical		Experimental			Analytical		Experimental			Analytical		Experimental		
r	χ	Eq. (40)	Eq. (44)	Al	Teflon	FR4	Eq. (40)	Eq. (44)	Al	Teflon	FR4	Eq. (40)	Eq. (44)	Al	Teflon	FR4
0.2	0.1	0.995	0.870	0.928	0.889	0.908	0.998	0.870	0.951	0.928	0.934	0.998	0.870	0.971	0.927	0.928
	0.2	1.000	1.000	1.000	1.000	1.000	1.000	1.000	1.000	1.000	1.000	1.000	1.000	1.000	1.000	1.000
0.4	0.1	0.988	0.757	0.902	0.841	0.875	0.995	0.757	0.913	0.885	0.879	0.997	0.757	0.928	0.902	0.905
	0.2	0.991	0.870	0.950	0.905	0.93	0.996	0.870	0.936	0.920	0.923	0.998	0.870	0.948	0.928	0.920
	0.3	0.994	0.944	0.984	0.966	0.973	0.997	0.944	0.967	0.957	0.958	0.998	0.944	0.967	0.964	0.963
	0.4	1.000	1.000	1.000	1.000	1.000	1.000	1.000	1.000	1.000	1.000	1.000	1.000	1.000	1.000	1.000
0.6	0.1	0.983	0.698	0.923	0.841	0.885	0.993	0.698	0.890	0.866	0.872	0.996	0.698	0.938	0.920	0.922
	0.2	0.985	0.802	0.940	0.893	0.915	0.994	0.802	0.910	0.893	0.901	0.997	0.802	0.955	0.953	0.938
	0.3	0.988	0.870	0.967	0.932	0.947	0.995	0.870	0.938	0.917	0.920	0.997	0.870	0.970	0.957	0.964
	0.4	0.990	0.922	0.980	0.962	0.968	0.996	0.922	0.964	0.959	0.948	0.998	0.922	0.977	0.969	0.960
	0.5	0.994	0.964	0.994	0.983	0.996	0.997	0.964	0.986	0.986	0.976	0.999	0.964	0.983	0.976	0.982
	0.6	1.000	1.000	1.000	1.000	1.000	1.000	1.000	1.000	1.000	1.000	1.000	1.000	1.000	1.000	1.000
0.8	0.1	0.979	0.659	0.851	0.751	0.813	0.991	0.659	0.895	0.843	0.856	0.995	0.659	0.904	0.887	0.874
	0.2	0.982	0.757	0.882	0.824	0.848	0.992	0.757	0.907	0.89	0.891	0.996	0.757	0.928	0.920	0.905
	0.3	0.985	0.821	0.923	0.875	0.894	0.994	0.821	0.923	0.907	0.914	0.997	0.821	0.935	0.928	0.932
	0.4	0.988	0.870	0.946	0.917	0.943	0.995	0.870	0.944	0.928	0.922	0.997	0.870	0.951	0.942	0.948
	0.5	0.991	0.910	0.977	0.951	0.964	0.996	0.910	0.960	0.948	0.954	0.998	0.910	0.963	0.958	0.958
	0.6	0.994	0.944	0.990	0.971	0.982	0.997	0.944	0.976	0.967	0.970	0.998	0.944	0.983	0.980	0.971
	0.7	0.996	0.973	0.992	0.990	0.992	0.998	0.973	0.988	0.976	0.980	0.999	0.943	0.991	0.984	0.983
	0.8	1.000	1.000	1.000	1.000	1.000	1.000	1.000	1.000	1.000	1.000	1.000	1.000	1.000	1.000	1.000

nearly 5% as the value of γ increases from 0.2 to 1.0. For the case of Teflon as a plate material, the discrepancy between experimental data and analytical results due to Eq. (44) at a particular value of χ is minimum (less than 10%) for the lowest value of γ. However, toward the highest value of γ, for experimental data and analytical results due to Eq. (40) the discrepancy is found to be a minimum for aluminum as a plate material (less than 11%).

V. Experimental Uncertainty Analysis

Because of a minor fluctuation in the ambient condition and complexity in the measurement and control of heater powers to maintain desired thermal conditions at various sections of the test plate, it was not possible to perfectly replicate the mix heating condition for a different test specimen. However, the tests were repeated and it was found that the maximum difference between any temperature level and its average value was 3.1%, 3.8%, and 4.1% for aluminum, Teflon, and FR4, respectively. The corresponding difference between any heat flux level and the average value was below 2.1%, 3.4%, and 4.4% for three plate materials in the same order. Heat loss by radiation from the heated surface was assumed to be less than 5% [13]. The uncertainty in the calculated quantities was determined according to the procedure by Moffat [15]. Analysis indicated less than a 6% uncertainty in surface heat flux measurements. Experimental uncertainty is based on a 95% confidence level.

VI. Conclusions

The conjugate heat transfer problem was investigated both analytically and experimentally for a vertical plate with natural convection at the surface and conduction below considering thermally thin wall regime approximation. Thermal specifications at the plate surface were a combination of UHF and UWT conditions. Comparative analysis is presented for the first order analytical solution for dimensionless temperature (at the UHF surface) and dimensionless heat flux (at the UWT surface) for the limiting case of $\alpha \to \infty$ with the experimental data for three values of α; that is, 1.178, 1.09×10^{-3}, and 1.636×10^{-3}. Analytical solution for dimensionless temperature for the limiting case of $\alpha \to 0$ was also presented and compared with experimental data. A reasonably good agreement was observed for normalized heat flux values with corresponding experimental data and therefore the analytical results for the limiting case of $\alpha \to \infty$ can be practically used for α values up to an order of magnitude 10^{-3}, and in doing so the magnitude of error will be less than 9%. Fair agreement was also observed for analytical solutions for dimensionless temperature for the two limiting cases. However, solution for the limiting case of $\alpha \to 0$ resulted in values within 10% of the experimental data for α with an order of magnitude 10^{-3}; and for the limiting case of $\alpha \to \infty$ gave better predictions (within 11%) for α values up to an order of magnitude near unity.

Acknowledgments

The authors gratefully acknowledge the efforts of V. Raghuram, Senior Research Engineer of the Department of Mechanical Engineering, IIT-Kanpur; P. S. Chauhan, Instrumentation Engineer of the Department Chemical Engineering, IIT-Kanpur; and Sushil K. Mishra, Senior Technical Assistant of the Heat Transfer Laboratory in the Department of Mechanical Engineering.

References

[1] Vallejo, A., and Trevino, C., "Convective Cooling of a Thin Plate in Laminar and Turbulent Flows," *International Journal of Heat and Mass Transfer*, Vol. 33, No. 3, 1990, pp. 543–554.

[2] Mendez, F., and Trevino, C., "The Conjugate Conduction-Natural Convection Heat Transfer Along a Thin Vertical Plate with Non-Uniform Internal Heat Generation," *International Journal of Heat and Mass Transfer*, Vol. 43, No. 15, 2000, pp. 2739–2748.

[3] Naylor, D., Floryan, J. M., and Tarasuk, J. D., "A Numerical Study of Developing Free Convection Between Isothermal Vertical Plates," *Journal of Heat Transfer*, Vol. 113, No. 3, 1991, pp. 620–626.

[4] Yadav, V., and Kant, K., "Convective Cooling of a PCB Like Surface with Mixed Heating Conditions in a Vertical Channel," *Journal of Electronic Packaging* (to be published).

[5] Trevino, C., and Linan, A., "External Heating of a Flat Plate in a Convective Flow," *International Journal of Heat and Mass Transfer*, Vol. 27, No. 7, 1984, pp. 1067–1073.

[6] Chen, T. S., Tien, H. C., and Armaly, B. E., "Natural Convection on Horizontal, Inclined and Vertical Plates with Variable Surface Temperature or Heat Flux," *International Journal of Heat and Mass Transfer*, Vol. 29, No. 10, 1986, pp. 1465–1478.

[7] Kazansky, S., Dubovsky, V., Ziskind, G., and Letan, R., "Chimney-Enhanced Natural Convection from a Vertical Plate: Experiments and Numerical Simulators," *International Journal of Heat and Mass Transfer*, Vol. 46, No. 3, 2003, pp. 497–512.

[8] Sparrow, E. M., Garcia, A., and Chuck, W., "Turbulent Duct Flow with Streamwise Nonuniform Heating at the Duct Wall," *International Journal of Heat and Mass Transfer*, Vol. 30, No. 1, 1987, pp. 175–185.

[9] Chen, L., Tian, H., Li, Y., and Zhang, D., "Experimental Study on Natural Convective Heat Transfer from a Vertical Plate with Discrete Heat Sources Mounted on the Back," *Energy Conservation and Management*, Vol. 47, Nov. 2006, pp. 3447–3455.

[10] Pozzi, A., and Lupo, M., "The Coupling of Conduction with Laminar Natural Convection Along a Flat Plate," *International Journal of Heat and Mass Transfer*, Vol. 31, No. 9, 1988, pp. 1807–1814.

[11] Merkin, J. H., and Pop, I., "Conjugate Free Convection on a Vertical Surface," *International Journal of Heat and Mass Transfer*, Vol. 39, No. 7, 1996, pp. 1527–1534.

[12] Kays, W. M., and Crawford, M., *Convective Heat and Mass Transfer*, McGraw–Hill, New York, 1980.

[13] Yadav, V., "Thermal Modeling of Electronic Packages Subjected to Buoyancy Assisted Convective Cooling in Air," Ph.D. Dissertation, Indian Institute of Technology, Kanpur, India, 2005.

[14] Shu, J. J., and Pop, I., "On Thermal Boundary Layers on a Flat Plate Subjected to a Variable Heat Flux," *International Journal of Heat and Fluid Flow*, Vol. 19, Feb. 1998, pp. 79–84.

[15] Moffat, R. J., "Describing the Uncertainties in Experimental Results," *Experimental Thermal and Fluid Science*, Vol. 1, No. 1, 1988, pp. 3–17.